Residual Stress Measurements of Cr-Coated Cladding

Nuclear Technology Research and Development

Prepared for
U.S. Department of Energy
Tim Graening
Mackenzie Ridley
Jesse Werden
Kory Linton
Nathan Capps
Oak Ridge National Laboratory

01/31/2024
M3FT- 24OR0202020411
ORNL/SPR-2024/3218

SUMMARY

Accident-tolerant fuel concepts for light-water reactor applications have been developed and tested in diverse research programs around the world. Industry teams have developed coated cladding concepts using different coating application methods, such as physical vapor deposition and coldspraying. Recently, variations in thickness and application method were investigated, and their effects on the microstructure and mechanical properties were reported. The results suggest an increase in performance in an unirradiated state, however, it remains unclear what phenomenon drove this performance. One explanation to this performance is associated with the coating process imparting a residual stress. Residual stress analysis was performed on coatings produced with various process parameters to understand how a thin layer of Cr impacts the mechanical properties after coating application and after simulated operating conditions. The gathered information is intended to address safety concerns or support margin identification related to accident-tolerant fuels and to support subsequent modeling and simulation efforts.

CONTENTS

FIGURES

TABLES

ACRONYMS

ASTM	ASTM International (formerly American Society for Testing and Materials)
ATF	accident-tolerant fuel
BSE	backscattered electron
EBSD	electron backscatter diffraction
HiPIMS	high-power impulse magnetron sputtering
LOCA	loss-of-coolant accident
ORNL	Oak Ridge National Laboratory
PVD	physical vapor deposition
PWR	pressurized water reactor
SEM	scanning electron microscopy
STEM	scanning transmission electron microscopy
TEM	transmission electron microscopy
XRD	x-ray diffraction
Zry-4	Zircaloy-4

1. INTRODUCTION

The Fukushima accident illuminated a need to increase research and development efforts on accident-tolerant fuels (ATFs) [1–3]. Different ATF concepts have been developed during the past decade, and efforts have been expended on both novel fuel and cladding ATF concepts. The primary goal of ATF development activities is to extend the coping time during a beyond-design-basis accident as well as to enhance safety and economic viability of nuclear reactors during steady-state operation and design-basis accidents (e.g., a loss-of-coolant accident [LOCA]). In practice, this goal is typically realized by ATF's improved high-temperature performance. Coating concepts, such as the application of a thin coating of highly corrosion-resistant material on the cladding's surface, have been investigated. One primary criterion for selecting the coating thickness and material is to ensure the coating does not diminish existing neutronic, thermal hydraulic, and mechanical performance under normal operating and transient conditions. Different coating materials, thicknesses, coating processes, process parameters, and testing methods have been developed, leading to new methods to investigate coated cladding material properties and mechanical performance [4–8]. Although some compositional variations in coatings are observed in the literature, Cr coatings were chosen for this study because of their outstanding corrosion resistance under normal operating temperatures and their high-temperature steam oxidation resistance under accident conditions. A clear concern for protective coatings in extreme environments is the reliability of coating processing and its effects on the cladding material during normal operation and accident scenarios. Understanding the effects of coating application parameters and simulated operating conditions on the Cr-coating is required to predict how a thin coating affects the bulk properties of the cladding material. Here, residual stress introduced during the coating application process on cladding tubes is investigated. That information can inform simulation efforts, when microstructural and mechanical data are combined to perform lifetime and accident scenario predictions.

2. MATERIALS AND METHODS

2.1 Cladding and Coating

The US Department of Energy's Oak Ridge National Laboratory (ORNL) procured several hundred meters of Zircaloy-4 (Zry-4) from Cameco Fuel Manufacturing (Port Hope, Ontario, Canada) in FY 2020. The material was stress relieved and conformed to the typical geometry of a pressurized water reactor (PWR) cladding, conforming to the ASTM International (ASTM) B353-12 standard. The nominal chemical composition of uncoated samples and dimensions are listed in Table 1.

Table 1. Dimensions and nominal chemical composition of Zry-4

Parameter	Zry-4[b]
Length (mm)	30.48
Width (mm)	9.50
Thickness (mm)	0.56
Zr (wt %)	Balance
Sn (wt %)	1.20–1.45
Fe + Cr + Ni (wt %)	0.37 (no Ni)
Cr (wt %)	0.07–0.13
Ni (wt %)	—

[b]ASTM B353

A dense, 6 to 9 μm thick Cr coating was applied to the Zry-4 cladding because Cr can provide a high-temperature corrosion benefit (e.g., act as a barrier to steam oxidation and loss of mechanical strength of

the Zry-4 substrate) while minimally affecting the composite tube's baseline mechanical performance. Before coating, the tubes' surfaces were polished by APEX grinding company to reduce the surface roughness down to 8 Ra.

The final outer diameter of the tubes was between 9.25 and 9.60 mm and was recorded for each tube before testing. Figure 1 shows the microstructure of the bare Zry-4 tubes in the axial and radial directions using inverse pole figure maps along with nanohardness measurement results. Unidentified regions (in white) in the inverse pole figure maps boast high dislocation densities and nanosized grains, typical for non-recrystallized regions. The coating microstructures for all tested materials have been reported in publicly available reports and are listed in Table 2.

Table 2. Sample description of produced and used samples for residual stress analysis

Sample name	Coating thickness (µm)	Comments	Reference
-90V Nov22 – batch 1	9.0	−90 V substrate bias, same process as 100 V batch 1	[9]
-90V Nov22 – 500h	9.0	Tested in autoclave for 500 h	[9]
-90V Nov22 – 1000h	9.0	Tested in autoclave for 1,000 h	[9]
-90V Nov22 – 1500h	9.0	Tested in autoclave for 1,500 h	unpublished
-90V Nov22 – 2000h	9.0	Tested in autoclave for 2,000 h	unpublished
-90V Apr23 – batch 2	9.1	Same process parameters as -90 V Nov22 – batch 1	unpublished
-100V bias batch 1*	5.5	−100 V substrate bias	[10,11]
-100V bias batch 2	7.3	Lower peak current during HiPIMS than batch 1	[11]
-150V bias*	6.2	−150 V substrate bias	[10,11]
-200V bias*	6.3	−200 V substrate bias	[10,11]
Coldsprayed Cr	31	Produced at Wisconsin University	[11]

*produced on the same day using the same batch process
HiPIMS = high-power impulse magnetron sputtering

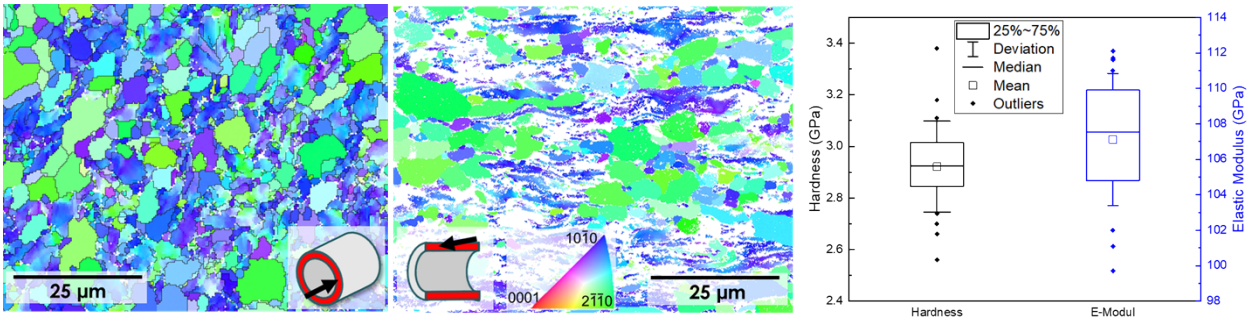

Figure 1. Microstructure of Zry-4 alloy tubes in (left) axial direction and (center) radial direction shown by via an inverse pole figure evaluated in axial direction of the tube. (right) Hardness and E-Modulus plots.

All physical vapor deposition (PVD) coatings were applied at Acree Technologies Inc. in California. Before the 12 in. Zry-4 tubes were mounted in a PVD coating machine, the tubes were cleaned using an ultrasonic cleaner and isopropanol. The application temperature was about 200°C, and a growth rate of between 1 and 2 nm/min was achieved, depending on the applied substrate bias. The relatively low coating temperature was chosen to ensure that thermal expansion differences between the Cr coating and the Zry-4 cladding material do not reduce the bonding strength. The coating process variables necessary to achieve a dense coating with a thickness of around 6 to 9 µm are reported in the literature [12–14].

2.2 X-Ray Diffraction Method

X-ray diffraction (XRD) was performed to investigate the change of the residual stress in the coating. Residual stresses are the sum of elastic and plastic deformation of crystallites across multiple scales: (1) macroscopic, where stresses are averaged across multiple grains (σ_I), (2) mesoscopic, as the average stress inside a single grain (σ_{II}), and (3) microscopic, as the fluctuation of stress inside a single grain (σ_{III}). Mechanical properties are defined mostly by the macroscopic stresses, which can get evaluated using x-rays analysis assuming a uniform and isotropic distribution of crystals. Stresses inside a sample lead to changes of the interplane distances d_{hkl}, which depends on the orientation of the grain inside the polycrystal. As shown in Figure 2, the interplane distance can be determined using x-ray scattering by Bragg's law [15]:

$$2d_{hkl}\sin\theta_{hkl} = n\lambda\,,$$

where θ_{hkl} is the Bragg angle for reflection, n is the diffraction order (1,2, or 3), and λ is the wavelength. For a set wavelength, the position of the diffraction peak can be calculated for each scattering lattice plane, where d^0_{hkl} is the unstrained, non-stressed lattice spacing. Therefore, the elastic deformation is given by the following equation:

$$\varepsilon^{hkl} = \frac{d_{hkl} - d^0_{hkl}}{d^0_{hkl}}.$$

The strain value of a stress tensor is given by $\varepsilon_{ij}(r)$, which is connected via a local compliance tensor $s_{ijkl}(r)$ to the residual stress using Hooke's law:

$$\varepsilon_{ij}(r) = s_{ijkl}(r)\sigma_{kl}(r).$$

Under the assumption of uniform isotropic grains in a polycrystal, the macroscopic stresses inside a specific material the local compliance tensor can be reduced to two parameters S_1 and S_2:

$$\varepsilon_{ij} = S_{ijkl}\sigma_{kl} = \left[S_1\delta_{ij}\delta_{kl} + \frac{1}{2}\,S_2\frac{\delta_{ik}\delta_{jl} + \delta_{il}\delta_{jk}}{2}\right]\sigma_{kl}.$$

The parameters can be expressed using the bulk properties of a material—the Young's modulus (E) and Poisson ratio (ν):

$$S_1 = -\frac{\nu}{E};\quad \frac{1}{2}S_2 = \frac{1+\nu}{E}.$$

The present "sample" coordinate system, the crystallographic and the laboratory coordinate system can be transferred to each other using transformation tensors. This process is not further discussed here; details are available in the literature [16]. For the present research, the ψ angle shown in Figure 2 is varied, while the not shown ϕ angle describing the rotation around the normal direction axis of the sample surface does not vary. The resulting fundamental equation of x-ray stress analysis is given by the following [16]:

$$\varepsilon_{\psi\phi}^{hkl} = \frac{1}{2}S_2 \sin^2\psi\left[\sigma_{11}\cos^2\phi + \sigma_{12}\sin 2\phi + \sigma_{22}\sin^2\phi - \sigma_{33}\right] + \frac{1}{2}S_2 \sin 2\psi\left[\sigma_{13}\cos\phi + \sigma_{23}\sin\phi\right] + S_1(\sigma_{11}+\sigma_{22}) + \sigma_{33}\left(\frac{1}{2}S_2 + S_1\right)$$

However, instead of relying on the accurate determination of each of the angles and values, the $\sin^2\psi$ method is used here. This method releases the sample shape and boundary conditions, leading to a tensor with only diagonal values. In that case, the values σ_{11} and σ_{22} can be determined from the inclination of the line fit at different $\sin^2\psi$ angles with a set $\phi = 0°$ and $\phi = 90°$, respectively. The term σ_{33} can be evaluated from the intersection with the ordinate. Here, the set ϕ angles of 0° and 90° are called axial and perpendicular orientations, respectively, as shown in Figure 3.

All the x-ray acquisition was performed using an x-ray diffractometer by Rigaku SmartLab equipped with a D/Tex detector. The instrument has no monochromator and uses a Cu radiation source with a 2:1 mixture of $K_{\alpha1}$ (λ_1 = 1.5406 Å) and $K_{\alpha2}$ (λ_2 = 1.54439 Å). All measurements were performed in parallel beam geometry. An initial scan was conducted on each sample between 30° and 120° of the 2θ range to identify qualifying peaks for residual stress analysis. An initial Bragg scan with a $\psi = 0°$ angle was performed to measure the potential shift of the peak position for the {*hkl*} plane fulfilling the Bragg condition with the normal for the {*hkl*} plane parallel to the sample surface.

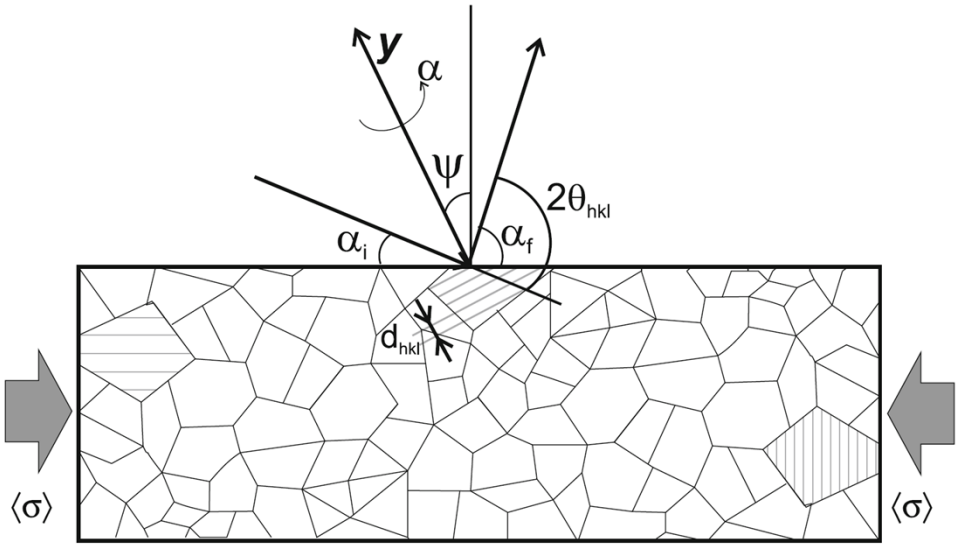

Figure 2. Schematic overview of x-ray diffraction inside a polycrystalline sample (Reprinted from Luo 2022 [16]).

2.3 X-Ray Diffraction Testing Parameters

Soller slits of 0.25° and a length-limiting slit were adjusted to each orientation of the sample to limit the curvature of the investigated area, as shown in Figure 3. A step size of 0.05° and a scan speed of 0.5°/min were selected for all scans. Also chosen were 0D-scans with an iso-inclination with fixed ψ angles with 11 points for ψ. The incident and first receiving slit were set to 1 and 2 mm, respectively, and the second receiving slit was completely open. These parameters worked well to obtain a distinct peak-to-noise ratio for Cr coatings. The coatings were measured with the tube axis perpendicular to the incident x-rays on the outside of the tube. The applied diffraction conditions and linear absorption coefficient of K_α-Cu in Cr and Zry-4 resulted in an x-ray depth penetration to the surfaces between 5.43 and 5.92 µm for 50° and 60° θ for Cr, and between 9.13 and 10.20 µm for 45° and 50° θ for Zr. Due to the lower penetration depth in Cr and

an average coating thickness of around 9 µm, the residual stress in the Zry-4 layer needed to be measured on a cut surface with the normal direction (axis 3 in Figure 2) parallel to the axial direction of the tube. However, this orientation was not feasible for the coating because the peak-to-noise ratio was not high enough to obtain reliable results. All the acquired diffraction data were processed by $K_{\alpha 2}$ stripping and background removing. Data smoothing of a five-point weighted average was used, before a peak search with the center of the full width half maximum of the peak was performed. In the stress calculation, the elastic modulus and Poisson's ratio were adapted as 140 GPa and 0.22, respectively, for Cr and as 107 GPa and 0.37, respectively for Zry-4 [17]. The *hkl* lattice plane {211} peak at 96.09° 2θ for Zry-4 and *hkl* {310} diffraction peak at 115.35° 2θ position for Cr (310) were chosen as lattice planes of interest because no overlapping peaks would interfere with increasing ψ angles, and a reliable peak-to-noise ratio could be obtained. Values from the Inorganic Crystal Structure Database file 625717 were used for Cr.

Literature values for the unstressed plane spacing were used as the d^0_{hkl} values. This assumption should lead to a measuring error of less than 0.1%. The present θ angles are also high enough to provide no artificially increased residual stress values, as observed in preliminary scans at lower 2θ positions reported in the literature [18].

However, the orientation for Zr, as shown in Figure 3 led to a curved area, resulting in measured residual stress values with a high deviation. This result indicates a more complex residual stress tensor that was not captured here.

To summarize, the ψ angle was changed throughout several x-ray scans, yielding different Cr grains with the same *hkl* plane oriented to the sample surface to scatter under Bragg's law. The shift of the 2θ position for differently oriented grains was recorded in regard to $\sin^2\psi$, which enables the calculation of the average planar stress in the tested volume.

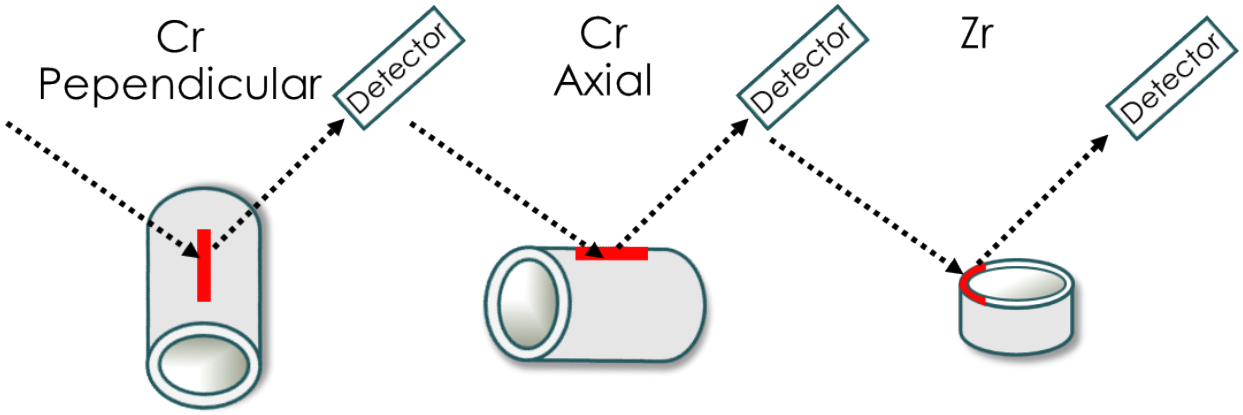

Figure 3. Orientation of tested tube samples depending on coating or cladding material.

2.4 Pressurized Water Testing

Specimens were exposed to prototypic PWR conditions in the absence of irradiation. A Ni-alloy autoclave was used to hold specimens in a 316 SS basket for exposure at 15.6 MPa and 330°C for 500 h increments. Continuous-flow deionized water was filtered to remove residual impurities, and hydrogen gas was introduced to the water supply to achieve a measured dissolved oxygen concentration below 5 ppb. Specimens were exposed to up to 2,000 h total exposure time.

2.5 Loss-of-Coolant Accident Testing

LOCA testing in the absence of irradiation was performed on 3 in. Zry-4 and Cr/Zry-4 cladding segments. Previous LOCA testing has shown that Cr-coated Zry-4 specimens display an increased resistance to

cladding rupture compared with uncoated Zry-4 [19]. The results of the current study on residual stresses from Cr deposition encouraged additional LOCA testing on coated cladding segments that have undergone stress relief annealing conditions. Here, specimens were first annealed in a vacuum furnace at 500°C for 1 h at 6×10^{-6} Torr total pressure to apply a stress-relief anneal to the Cr-coated Zry-4 cladding segment. For appropriate comparison, the Zry-4 uncoated segment was also annealed under the same conditions. Details on the LOCA test setup can be found elsewhere [20]. Tubes were painted with high-temperature paint on the outer diameter surface for in situ deformation tracking with 3D digital image correlation. Segments were connected to a high-pressure line with Swagelok fittings and placed within the four-lamp infrared heating furnace. Thus, specimens were internally pressurized with Ar (gas) to 9.65 MPa at room temperature, and pressure was held constant to the gas cylinder pressure reservoir. Each segment was heated to 100°C, and then steam was flown around the exterior of the cladding. Next, each segment was heated to 300°C for 5 min to provide a temperature equilibration near the expected operating temperatures of cladding in a reactor. The LOCA test initiated with a 5°C/s heating rate from 300°C until cladding rupture.

3. RESULTS

3.1 X-Ray Diffraction Residual Stress Evaluation

An example of a single 2θ–sin 2ψ plot is shown in Figure 4 for the −100 V bias Cr coating (Table 2). A linear function was used to fit the results with very low deviations, indicating a diagonal stress tensor. If instead of a linear fit, an oscillating function or a parabolic function would result in a higher reliability, then the presence of a strong texture or a strong stress component along the normal radial direction of the tube, respectively, would be indicated. Most of these results could be fitted very well using a linear approximation, except for the −150 V bias coating, because the adhesion of the coating made a measurement difficult: an unwanted ablation of the coating occurred during the surface cleaning process. The measurements of that coating are not reported. Another sample exhibiting a larger deviation was the "-90V Apr23" sample. Two measurements were performed here, and the average of both measurements from two different tubes is shown in Figure 5. Microscopy investigation of that batch did not reveal a difference to the anisotropic behavior of the previous "-90V Nov22" batch.

Residual stress inside a material can increase or decrease its macroscopic mechanical properties. This change triggered the investigation of the residual stress in coated cladding in the first place. The XRD residual stress measurement results for Cr in as-produced conditions for samples displayed in Table 2 are shown in Figure 5.

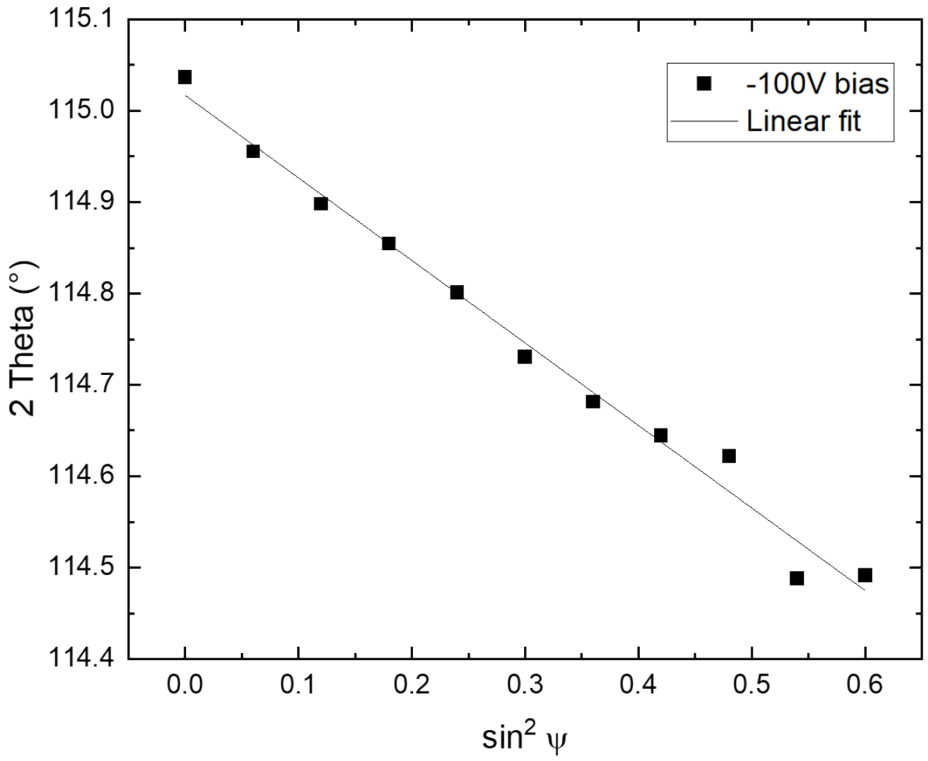

Figure 4. Plot of 2θ with respect to $\sin^2\psi$ for the −100 V substrate bias batch 1 material in the axial direction.

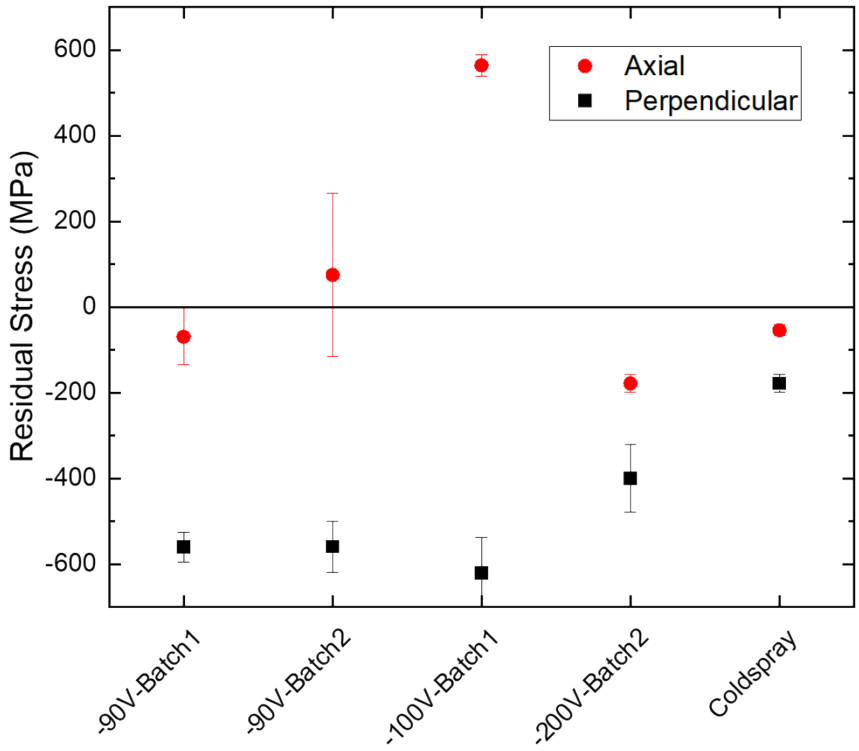

Figure 5. Residual stress values determined for axial and perpendicular measurement conditions from different PVD and coldsprayed coatings.

Independent of the coating condition, a compressive residual stress in the perpendicular direction was recorded, whereas a slightly negative or unstressed tensor component in the axial direction was measured for most samples. The major deviation from that observation is the coating "-100V bias batch1," which showed a non-negatable tensile stress in the axial direction of 564 MPa. Although the exact same processing parameters between the shown "-90V Nov22 batch1" and "-90V Apr23 batch2" were used to manufacture the coating, the measured residual stress shows slight deviations. The "-100V bias batch1" was manufactured under the same process parameters as the two mentioned −90 V batches, with a slight difference of 10 V in the substrate bias, but that detail cannot explain the spike in the repeatably measured tensile stress in the as-coated condition. By contrast, the "100V Batch-2" did not give conclusive results: the coating was less homogenous as previously reported in the microstructure, resulting in an oscillating fit that cannot be interpreted with the current XRD setup. Another important observation can be made: comparing the present results with the previously reported burst test results reveals an increase of burst temperature of around 50°C for the "100V-batch1" and the coldspray coatings. However, the calculated residual stress of both coatings results in very different values in both measurement directions. The "-100V-Nov22-batch1" sample proves that a strong axial tension stress inside the Cr coating introduces a compressive response in the Zry-4 cladding material (assuming a good bonding strength as demonstrated).

The same explanation cannot be made for the low residual stress component values for coldsprayed materials. However, the extinction length of the wavelength used inside the Cr layer is around 6 µm, so only the surface part of the coldsprayed coating was investigated. Thus, the investigated region inside the coldsprayed material is not representative for the entire coating thickness, and a future depth-sensitive investigation is required for this material.

Therefore, a comparison between various high-power impulse magnetron sputtering (HiPIMS) Cr-coated materials with coating thicknesses between 5.3 and 7.2 µm should be more reasonable. Nevertheless, the low extinction length of the x-rays can cause a significant inaccuracy in comparison across different

thicknesses. Therefore, Cr-coated samples from an autoclave experiment to simulate reactor operating conditions conducted in FY 2023 were examined ex situ to investigate the residual stress development after different exposure times inside the autoclave. The thermal stress, owing to the different coefficients of thermal expansion between Cr and Zr, is neglectable in comparison when only different autoclave times are considered. Instead, the residual stress anneals slowly under those conditions, affecting each stress component inside the tensor differently. Figure 6 shows these results: the residual stress is plotted against the exposed time in the autoclave.

Interestingly, the compressive stress in as-coated condition of the "-90V-Nov22-batch1" coating changes over time. Within the first 500 h, the change is within the margin of error, but with longer holding times at operating temperatures, the strong compressive stresses decrease by around 154 MPa, while the other stress component measured in the axial direction increases by more than 200 MPa. These results clearly demonstrate the long-term change of the coating inside an operating reactor, with changes in the resulting microstructure, as polygonization occurs. These changes are unlikely to be measurement errors because the same material was used for all tests illustrated in Figure 6. However, the burst behavior of material exposed to such conditions is unknown and must be explored. Furthermore, the present results challenge neutron irradiation's effect on residual stress—neutron irradiation is reported to anneal the residual stress out of the material even at low irradiation damage conditions of a couple displacements per atom.

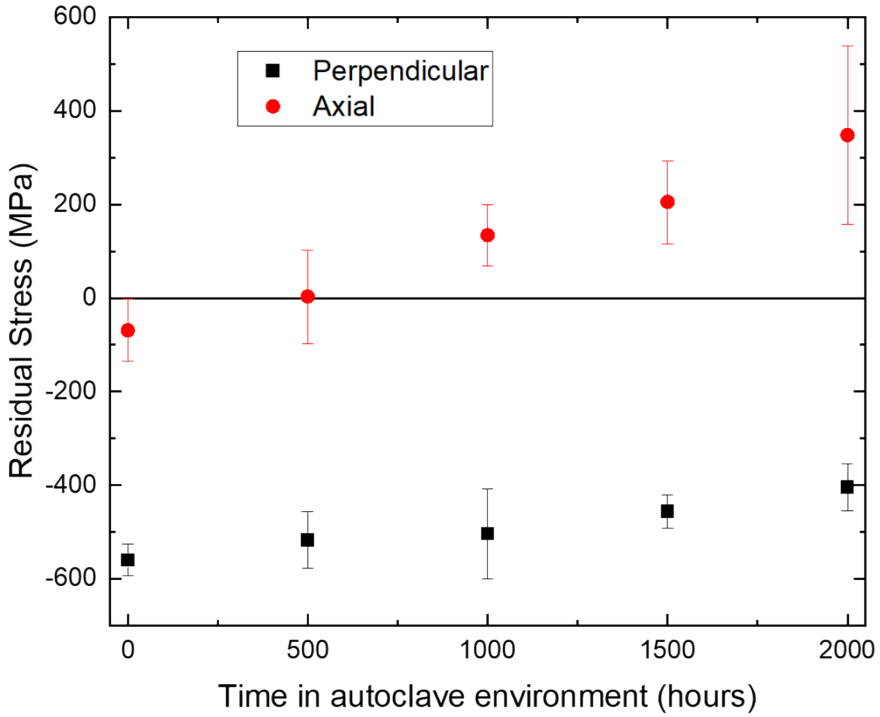

Figure 6. Determined residual stress in perpendicular and axial measuring condition of the "-90V-Nov22-batch1" sample.

3.2 Burst Test Results

Both Cr-coated and uncoated Zry-4 cladding segments showed similar rupture openings and rupture temperatures after LOCA testing. Figure 7 shows the camera images of each sample after rupture. Each sample had similar rupture opening geometries and sizes. Both images show the high-temperature paint speckle pattern that was used for deformation tracking in situ via stereo digital image correlation.

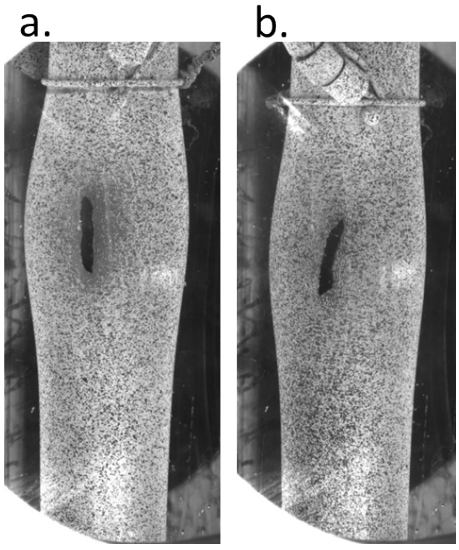

Figure 7. Rupture openings after 5°C/s LOCA testing for (a) uncoated Zry-4 and (b) Cr-coated Zry-4.

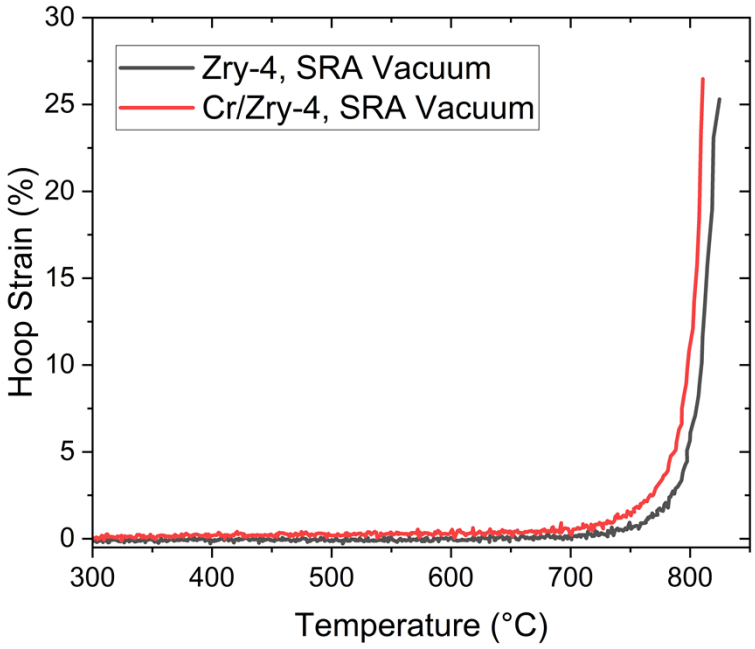

Figure 8. Average in situ deformation measurements from stereo digital image correlation during 5°C/s LOCA testing.

Figure 8 shows the average hoop strain across the visible regions of both specimens for the duration of the LOCA tests. Clearly, the Cr-coated Zry-4 cladding segment behaved similarly to the uncoated reference material after the stress relief anneal in the vacuum furnace. These results differ from what has been seen in the literature for LOCA testing of as-deposited Cr-coated Zry-4 cladding segments [REF], where Cr-coated material can showcase up to ~80°C increases in rupture temperature. The present results reveal that residual stress from the coating deposition process improves the mechanical performance of Cr-coated Zry-4 under accident scenarios. Consequently, residual stress retention during normal operating

temperatures and pressures and, most importantly, during irradiation are crucial concerns if the residual stresses are required for implementation of Cr-coated Zr alloys as a near-term ATF cladding option.

4. SUMMARY

Residual stress measurements of Cr-coated tubes produced via HiPIMS with different process parameters and coldspraying were conducted to evaluate the effect of a thin layer of Cr on the roughly 50 to 100 times thicker cladding material. The results show high stress values of up to 600 MPa for σ_{11} and σ_{22} stress components, which can affect the coating–cladding interface and cladding performance. Samples exposed in an autoclave were investigated, confirming the anticipated annealing process inside the material. This annealing process reduced the large compressive stress value in one measurement direction, alleviated by a slight showing of a tensile stress in the perpendicular direction. These reported values can be directly employed in simulation efforts for residual stress values σ_{11} and σ_{22}.

Burst testing of an annealed sample of a coated material, which previously showed an increase in burst temperature, did not show any difference between coated and uncoated material. This behavior challenges the notion that residual stress, as influential as it certainly on the interface and cladding material, has an insignificant contribution under effects such as neutron irradiation and long-term annealing under service conditions. Will the residual stress anneal out during commercial operation consisting of neutron irradiation and temperatures up to 400°C?

Therefore, a detailed study on neutron-irradiated material is required to help elucidate the interconnected mechanisms. Residual stress measurements with multiple slits to investigate larger volumes could be used to determine the residual stresses in larger ranges to calculate the triaxial terms. These measurements were not part of this initial screening of the residual stresses, but higher energies and shorter measurement times could help in the future to gain detailed local understanding of the intricacies between coating and cladding material.

5. REFERENCES

[1] M.N. Cinbiz, N. Brown, R.R. Lowden, M.N. Gussev, K.D. Linton, K.A. Terrani, Report on Design and Failure Limits of SiC/SiC and FeCrAl ATF Cladding Concepts under RIA, (2018).

[2] C. Tang, M. Stueber, H.J. Seifert, M. Steinbrueck, Protective coatings on zirconium-based alloys as accident-Tolerant fuel (ATF) claddings, Corros. Rev. 35 (2017) 141–165. https://doi.org/10.1515/corrrev-2017-0010.

[3] M. Kurata, Research and Development Methodology for Practical Use of Accident Tolerant Fuel in Light Water Reactors, Nucl. Eng. Technol. 48 (2016) 26–32. https://doi.org/10.1016/j.net.2015.12.004.

[4] T. Shinozaki, Y. Udagawa, T. Mihara, T. Sugiyama, M. Amaya, Improved-EDC tests on the Zircaloy-4 cladding tube with an outer surface pre-crack, J. Nucl. Sci. Technol. 53 (2016) 1426–1434. https://doi.org/10.1080/00223131.2015.1123658.

[5] T. Jezequel, Q. Auzoux, D. Le Boulch, M. Bono, E. Andrieu, C. Blanc, V. Chabretou, N. Mozzani, M. Rautenberg, Stress corrosion crack initiation of Zircaloy-4 cladding tubes in an iodine vapor environment during creep, relaxation, and constant strain rate tests, J. Nucl. Mater. 499 (2018) 641–651. https://doi.org/10.1016/j.jnucmat.2017.07.014.

[6] H. Li, T. Koyanagi, X. Hu, Y. Katoh, Multiscale experimental characterization of coatings on ceramics: A case study of tungsten on SiC, Surf. Coat. Technol. 367 (2019) 1–10. https://doi.org/10.1016/j.surfcoat.2019.03.040.

[7] J. Chen, S.J. Bull, Approaches to investigate delamination and interfacial toughness in coated systems: An overview, J. Phys. Appl. Phys. 44 (2011). https://doi.org/10.1088/0022-3727/44/3/034001.
[8] H. Chen, X. Wang, R. Zhang, Application and development progress of Cr-based surface coating in nuclear fuel elements: II. Current status and shortcomings of performance studies, Coatings 10 (2020). https://doi.org/10.3390/coatings10090835.
[9] T. Graening, M. Ridley, J. Werden, K. Linton, N. Capps, Impact of Flawed Coatings on the Microstructure under Relevant Operating Conditions.pdf, ORNL, Oak Ridge, n.d.
[10] T. Graening, K. Kane, B. Garrison, K. Linton, A. Nelson, Impact of Coating Defects on Performance of Coated Zirconium Cladding, 2021. https://doi.org/10.2172/1887714.
[11] T. Graening, M. Ridley, C. Massey, K. Linton, A. Nelson, Summarizing Effect of Coating Thickness and Condition on Behavior of Zr Cladding, ORNL/SPR-2022/2539, n.d.
[12] J.C. Brachet, I. Idarraga-Trujillo, M. Le Flem, M. Le Saux, V. Vandenberghe, S. Urvoy, E. Rouesne, T. Guilbert, C. Toffolon-Masclet, M. Tupin, C. Phalippou, F. Lomello, F. Schuster, A. Billard, G. Velisa, C. Ducros, F. Sanchette, Early studies on Cr-Coated Zircaloy-4 as enhanced accident tolerant nuclear fuel claddings for light water reactors, J. Nucl. Mater. 517 (2019) 268–285. https://doi.org/10.1016/j.jnucmat.2019.02.018.
[13] J. Brachet, M. Dumerval, M. Le Saux, E. Rouesne, S. Urvoy, T. Guilbert, Q. Houmaire, C. Cobac, Behavior of chromium coated M5TM claddings under loca conditions To cite this version : HAL Id : hal-02419638, WRFPM 2017 Water React. Fuel Perform. Meet. (2017).
[14] J. Ribis, A. Wu, J.C. Brachet, F. Barcelo, B. Arnal, Atomic-scale interface structure of a Cr-coated Zircaloy-4 material, J. Mater. Sci. 53 (2018) 9879–9895. https://doi.org/10.1007/s10853-018-2333-1.
[15] F.H. Chung, ed., Industrial applications of x-ray diffraction, Marcel Dekker, New York, 2000.
[16] A. Benediktovich, I. Feranchuk, A. Ulyanenkov, Theoretical Concepts of X-Ray Nanoscale Analysis: Theory and Applications, Springer Berlin Heidelberg, Berlin, Heidelberg, 2014. https://doi.org/10.1007/978-3-642-38177-5.
[17] L. Zhang, L. Dong, B.J. Nelson, Ring closure of rolled-up Si/Cr nanoribbons, Appl. Phys. Lett. 92 (2008) 143110. https://doi.org/10.1063/1.2906906.
[18] Q. Luo, S. Yang, Uncertainty of the X-ray Diffraction (XRD) sin2 ψ Technique in Measuring Residual Stresses of Physical Vapor Deposition (PVD) Hard Coatings, Coatings 7 (2017) 128. https://doi.org/10.3390/coatings7080128.
[19] M. Ridley, S. Bell, B. Garrison, T. Graening, N. Capps, Y.-F. Su, P. Mouche, B. Johnston, K. Kane, Effects of Cr/Zircaloy-4 coating qualities for enhanced accident tolerant fuel cladding, Ann. Nucl. Energy 188 (2023) 109799. https://doi.org/10.1016/j.anucene.2023.109799.
[20] M. Ridley, C. Massey, S. Bell, N. Capps, High temperature creep model development using in-situ 3-D DIC techniques during a simulated LOCA transient, Ann. Nucl. Energy 193 (2023) 110012. https://doi.org/10.1016/j.anucene.2023.110012.